



## NUMERICAL AND EXPERIMENTAL INVESTIGATION OF TUBE BUNDLE HEAT EXCHANGER ARRANGEMENT EFFECT ON HEAT TRANSFER PERFORMANCE IN TURBULENT FLOWS

Erman ASLAN\*, İmdat TAYMAZ\*\*, Kemal ÇAKIR\*\*\* and Elif EKER KAHVECİ\*\*\*\*

\* Kocaeli University, Engineering Faculty, Department of Mechanical Engineering  
41380, Kocaeli, erman.aslan@kocaeli.edu.tr, ORCID: 0000-0001-8595-6092

\*\* Sakarya University, Engineering Faculty, Department of Mechanical Engineering  
54050, Sakarya, taymaz@sakarya.edu.tr, ORCID: 0000-0001-5025-5480

\*\*\* Sakarya University, Engineering Faculty, Department of Mechanical Engineering  
54050, Sakarya, cakir@sakarya.edu.tr, ORCID: 0000-0003-2194-5567

\*\*\*\* Sakarya University, Engineering Faculty, Department of Mechanical Engineering  
54050, Sakarya, eeker@sakarya.edu.tr, ORCID: 0000-0001-6822-8296

(Geliş Tarihi: 28.02.2023, Kabul Tarihi: 16.06.2023)

**Abstract:** This study examines the friction factor, convective heat transfer, and area goodness factor of both inline and staggered tube bundles. The Finite Volume Method (FVM) is used for numerical simulations. Experimental and numerical approaches are utilized. Both 18.0 mm and 21.6 mm longitudinal distances are investigated. It is recommended to use ratio coefficients to reduce computation time. The proportion coefficients are used to obtain predictions for the three-dimensional cases based on the two-dimensional results or to transfer the 2D results to 3D. In addition, three turbulence models were utilized and compared within an Unsteady Reynolds Averaged Navier-Stokes (URANS) formulation. Experimental results validated numerical predictions. The thermal boundary conditions consist of a constant inlet temperature and a uniform heat flux on the support plate. Reynolds number is changed from 989 to 6352, while the Prandtl number remains at 0.70. Nusselt number and friction factor values have been observed to increase with increasing Reynolds number in all geometric configurations. The staggered configurations result in greater Nusselt number and friction factor values compared to inline configurations. The Nusselt number and pressure drop experience negative and positive effects, respectively, as the distance between rows decreases. SST turbulence models typically predict reasonable outcomes for all geometric configurations.

**Keywords:** Friction factor, Convective heat transfer, Tube bundle, Unsteady Reynolds averaged numerical simulations, Finite volume method.

## TÜRBÜLANSLI AKIŞLARDA ISI TRANSFER PERFORMANSI ÜZERİNDEKİ BORU DEMETLİ ISI DEĞİŞTİRİCİ SIRALAMA ETKİSİNİN SAYISAL VE DENEYSEL İNCELENMESİ

**Özet:** Düzgün ve kaydırılmış sıralı hatlara sahip boru demetlerinin sürtünme faktörü, taşınım ile ısı geçişi ve alan uyum faktörü özellikleri deneysel ve sayısal olarak incelenmiştir. Sonlu Hacim Yöntemi (FVM) kullanılmıştır. 18.0 mm ve 21.6 mm olmak üzere iki farklı uzunluğuna mesafe incelenmiştir. Daha az hesaplama için oran katsayılarının kullanılması önerilir. Oran katsayıları, iki boyutta elde edilen sonuçlara dayanarak üç boyutlu durumlar için tahminler elde etmek, başka bir deyişle 2B sonuçları 3B'ye aktarmak için uygulanır. Bir URANS (farklı Kararsız Reynolds Ortalama Navier-Stokes) formülasyonunda üç türbülans modeli kullanıldı ve birbirleriyle karşılaştırıldı. Sayısal tahminler deneysel sonuçlarla doğrulandı. Isıl sınır koşulu olarak, girişte sabit sıcaklık uygulanır ve destek plakasında üniform ısı akışı gerçekleşir. Reynolds sayısı 989'dan 6352'ye değiştirilmiş ve Prandtl sayısı 0.70'de tutulmuştur. Nusselt sayısı ve sürtünme faktörü değerleri tüm geometrik konfigürasyonlar için Reynolds sayısı ile artmıştır. Kaydırılmış sıralamalar, düzgün düzenlemeye kıyasla daha büyük Nusselt sayısı ve sürtünme faktörü değerlerine yol açmıştır. Nusselt sayısı ve basınç düşüşü, sıralar arasındaki boyuna mesafenin azalmasıyla sırasıyla negatif ve pozitif etkiye sahiptir. Genel olarak, SST türbülans modelleri, tüm geometrik konfigürasyonlar için makul sonuçlar vermiştir.

**Anahtar Kelimeler:** Sürtünme faktörü, Taşınım ile ısı geçişi, Boru demeti, Zamana bağlı Reynolds ortalamalı sayısal benzeşim, Sonlu hacimler yöntemi.

## NOMENCLATURE

$T_i$	inlet temperature, K
$T_0$	outlet temperature, K
$T_w$	average wall temperature, K
$F_{WA}$	heat transfer area, m <sup>2</sup>
$A_{GF}$	area goodness factor
$\Delta P$	pressure drop, N m <sup>-2</sup>
$Nu$	Nusselt number, dimensionless
$Re$	Reynolds number, dimensionless
$Pr$	Prandtl number, dimensionless
$f$	Friction factor
$\rho$	fluid density, kg m <sup>-3</sup>
$Q$	heat flow rate, J s <sup>-1</sup>
$k$	fluid (air) thermal conductivity, W m <sup>-1</sup> K <sup>-1</sup>
$h$	convective heat transfer coefficient, W m <sup>-2</sup> K <sup>-1</sup>
$D$	tube diameter, m
$U$	inlet velocity, m s <sup>-1</sup>
$\omega$	specific dissipation rate
$SST$	Shear Stress Transport
$\dot{m}$	mass flow rate, kg m s <sup>-2</sup>

## INTRODUCTION

Understanding and accurately determining the convective heat transfer coefficient on the tube bundle support plate is crucial for analysing different tube bundle arrangements in heat exchangers and similar systems. With the development of nuclear power plants, steam generators have assumed a crucial role. There are four distinct heating arrangements: helical steam generators, meander steam generators, straight-flow heat exchangers, and U-tube heat exchangers. The most prevalent design for steam generators is the spiral configuration. Different-sized spiral-wound tubes are nested within one another to create a compact cylindrical tube bundle. The tube bundle is positioned on the support plates, where thermal stresses occur. A precise understanding of the convective heat transfer coefficient between the gas and the plate is necessary for determining the structural integrity of supporting plates through stress analysis. In addition, precise knowledge of the fluid and thermal areas is required for the analysis of thermal/hydraulic and thermal/structural unit designs in large-scale heat exchangers for nuclear applications (Aburoma et al., 1975).

It is extremely difficult to locate expansive experimental areas. Consequently, during thermal and hydraulic experiments, a single geometric arrangement of a single tube or tube bundle has replaced large-scale heat exchangers. Experiments have provided valuable insights into the behaviour of the tube; however, obtaining a precise temperature profile is still difficult due to data limitations. The temperature field is affected by the configuration of the tube bundle and the flow distribution (Dagsoz, 1975). The model has been evaluated in order to determine the convective heat transfer coefficient between the support plate and the medium through which the gaseous fluid flows. Formation and separation of the boundary layer have a

substantial impact on heat transfer processes. By altering the flow patterns and thermal gradients at the surface, these phenomena have a significant effect on the efficiency of heat transfer. Cross-flow single-tube heat exchangers are rarely used in practise. Pipe bundles are utilised. Experiments are costly and time-consuming, so it is more practical to use numerical methods to calculate heat transfer coefficients than to conduct experiments (Aburoma et al., 1975).

In large heat exchangers, determining the pressure drop is equally as important as determining the convective heat transfer coefficient, as the pressure drop value affects directly the operating costs (Aburoma et al., 1975). When constructing a heat exchanger, a low pressure drop and a high heat transfer rate are considered ideal. In addition, reasonable operating costs are taken into account.

The tube bundle is arranged in a row and triangular shape, and the heat transfer coefficient is affected by these arrays. Hilpert (1933) devised a method for calculating the tube bundles' heat transfer coefficient. Grimison (1937) provides the constants formulated by Hilpert (1933). Brandt (1985) created an alternative method. This technique is the ratio of the volume between the tube bundles to the total volume of the bundle. In this research, both experimental and numerical studies are conducted. The literature review is therefore divided in half. Following a review of the experimental work, a review of the numerical research is provided. Kwak et al. (2003) investigated experimentally the convective heat transfer and penalty of pressure drop for an arbitrary number of transverse rows in a staggered finned tube with a single transverse row of the winglet pairs beside the front row of the tube bundles. In the experiments, two, three, four, and five rows of staggered tubes were used. The pair of wings used to improve heat transfer and reduce pressure loss were positioned in a manner that had not been used previously. Heat transfer increased by 30-10% in front of three rows of tubes along a single transverse row, while pressure loss decreased by 55-34%. Matos et al. (2004) conducted an experimental and numerical study to increase the total heat transfer rate between a finned tube bundle with staggered circular and elliptical tube arrangements. The optimal geometry for circular and elliptical tubes has been identified. The heat transfer gain in the ideal elliptical configurations was 19% greater than in the circular configurations. Kukulka and Smith (2014) conducted experimental research on tube bundles with staggered configurations. The use of Vipertex 1EHT enhanced heat transfer surface as opposed to smooth tubes, in conjunction with the use of various fluids such as n-Pentane, p-Xylene, and water, has resulted in a significant improvement in heat transfer capabilities. The Vipertex 1EHT tubes have been shown to increase heat transfer rates in comparison to conventional smooth tubes, making them a viable option for optimising heat transfer performance in a variety of applications. Ozturk et al. (2016) investigated the flow characteristics of a staggered array of multiple circular cylinders in a rectangular channel with close spacing.

PIV (laser particle image velocimetry) was utilised for this experiment. In experiments, a turbulent flow regime was identified. Distribution of velocity vector, streamline, vorticity and Reynolds stress, turbulent kinetic energy fields, and results from a single point spectral analysis were used to analyse flow characteristics in depth. Zhao et al. (2016) conducted an experiment to determine the pressure drop and friction factor values in the circular, elliptical, square, triangular, and diamond-shaped staggered array mini pins and the rectangular channel. Experiments were conducted with respect to three distinct flow regimes: laminar, transitional, and turbulent. It was observed that the friction factor correlation values could not accurately identify the entire flow region, including the laminar transition and turbulent regions, but correlations were still required. In additional experimental investigations, researchers have investigated a variety of variables in an effort to increase heat convection and reduce pressure drop. The utilisation of various tube shapes, such as elliptic (Khan et al., 2004; Ibrahim and Goma, 2009), twisted oval (Liu et al., 2018), and cam-shaped (Lavasani et al., 2014), has been investigated. These studies aim to optimise heat transfer performance by manipulating the tube geometry, resulting in enhanced convective heat transfer while minimising pressure drop within the system.

In addition, researchers have investigated the use of spherical turbulence promoters as an alternative configuration to improve heat transfer and reduce friction factor. Maithani et al. (2020) conducted a study on the application of spherical-shaped turbulence promoters, which revealed enhanced heat transfer performance and decreased friction factor. Utilising the unique flow characteristics induced by spherical turbulence promoters, this configuration maximises convective heat transfer while minimising energy losses due to friction within the system. They conducted experiments with Reynolds numbers ranging from 4500 to 16500. Various geometric parameters are defined, including the dimensionless spherical-shaped diameter, the stream-wise spacing parameter, and the span-wise spacing parameter.

Numerous instances exist in the literature for the numerical computation of heat convection on various configurations, without necessarily referring to the pressure drop. Some of these investigate laminar flow, including flow around a bluff body (Taymaz et al., 2015) and flow in a micro heat exchanger (Maqableh et al., 2011). Turbulent flow was considered for pipe flow (Benim et al,2004; You et al,2017), impinging jets (Chattopadhyay a Benim,2011; Benim et al,2007), flow around bluff bodies (Benim et al,2011) and elliptic tubes (Oclon et al,2015), gas turbine cooling (Benim et al,2004) and exhaust hood of steam turbines (Benim et al,1995). Launder and Massey (1978) conducted the first research on viscous laminar flow and heat transfer, referring to the pressure drop in the pipe bundle. To discretize the applied stream function-vorticity formulation, the finite difference method (FDM) was used. Barmasian and Hassan (1997) investigated flow characteristics in non-staggered and staggered tube

bundles for turbulent flow numerically using the Large Eddy Simulation (LES) method and two different sub grid scale closure models. Their findings were consistent with the experimental data (Oengoeren and Ziada, 1992). Beale and Spaulding (1999) utilised the Finite Volume Method (FVM) to examine the heat transfer and flow characteristics of unsteady fluid flow. In tube bundles, the ratio of pitch (range) to diameter was determined to be 2:1. The staggered calculation of Strouhal numbers was consistent with experimental data. Mizushima and Suehiro (2005) performed an analysis of the flow through two consecutive circular cylinders. FDM is utilised for numerical research. When the constant and symmetrical flow at low Reynolds numbers exceeds the critical Reynolds number, it becomes unstable and changes to the released flow. For time discretization, the Runge-Kutta method of the fourth order was used. On drag and lift coefficients, it was discovered that the distance between two consecutive cylinders is significant. Horvat et al. (2006) examined transition numerical simulations for flow and heat transfer analysis in cylindrical, ellipsoidal, and winged different shapes of staggered arrangements. Ansys commercial code (FVM) Ansys-CFD was used to simulate unsteady three-dimensional numerical simulations. The shear stress transport (SST) model was used to model turbulence. To prevent large mesh sizes, periodic boundary conditions were employed. Estimates were made for heat transfer, drag coefficients, and Stanton numbers. Experimental data are compatible with numerical results for all Re and tube shapes. Bouris et al. (2001) compared numerically the flow and heat transfer characteristics of three different tube configurations, namely elliptic-shaped tubes in inline arrangements, circular-shaped tubes in inline arrangements, and circular-shaped tubes in staggered arrangements. They demonstrated that inline arrangements with elliptical tubes produced high heat transfer values and low pressure drop values. Hamid et al. (2014) created a two-dimensional model of a pre-heater using CFD by analysing fluid flow and heat transfer in a circular and elliptical tube bundle. Lin et al. (2008) created a three-dimensional turbulence model to improve the heat transfer performance of plate-fin heat exchangers utilising two distinct vortex generators. After comparing annular and inclined blocks, the best heat transfer performance was observed in vortex generators with an inclined block shape. Mavridou and Bouris (2012) discussed a new cross-flow tube heat exchanger for investigating properties such as fluid flow and heat transfer and inline-ordered tubes of varying diameters. There were a total of three arrangements, and they were compared. The first was a bundle of tubes with a common row of equal-diameter cylinders; the others are two different arrangements with two different transverse spacing and a ratio of 0.5 between the diameters of the small and large cylinders. FVM was employed as the numerical technique. LES was used to model the turbulent flow regime. Utilising alternately positioned cylinders with a diameter of 0.5 increased heat transfer and decreased pressure drop. A CFD study of the flow and heat transfer quantities in the inline bundle of tubes was examined by Abed and Afgan (2017), using URANS

turbulence models, namely, a standard  $k-\epsilon$  model, SST  $k-\omega$ ,  $v2-f$  model, and EB  $k-\epsilon$  model. Two configurations, square and non-square inline, with variable vertical and horizontal aspect ratios, were used. The closest results were achieved by the EB  $k-\epsilon$  model, whereas the  $v2-f$  model also provided good results. Yahiaoui et al. (2016) investigated the change of flow characteristics around staggered tube bundles by the use of the grooved cylinders by using FVM with a Reynolds number of 9300, free stream velocity of 3.5 m/s, and pitch-to-diameter ratio of 3.8. Spalart–Allmaras,  $k-\epsilon$  realizable, and  $k-\omega$  SST, turbulence models were used. After the numerical analysis, it was in good agreement with the experimental results.

Another numerical investigation is done by Pourdel et al. (2019) for determining fluid flow and heat transfer in a flat tube under constant heat flux. In the numerical study Finite Volume method with SIMPLEC was used. The considered range of Reynolds numbers is 5000-20000, the range of dimensionless pitch is 1-2.33, and the range of dimensionless depth is 0.233-0.433. They observed that the presence of dimples inside of the channel changes the flow physics, temperature field, and heat transfer enhancement significantly in a good manner. For turbulence modeling, SST  $k-\omega$  was used. Zheng et al. (2020) investigated the effects of morphology variation, wall temperature, transverse pitch, and longitude pitch of the tube bundle on ash deposition and heat transfer performance under high-temperature conditions by using a dynamic simulation method based on ANSYS FLUENT.

This paper investigates experimentally and numerically the effect of longitudinal distance between tubes on convective heat transfer friction factor and area goodness factor for flow over tube bundle arrangements (inline and staggered) on the support plate. In numerical calculations, the commercial code Ansys-Fluent (2009) based on FVM is utilised. To reduce computational effort, proportion coefficients are proposed for Nusselt number and pressure drop for all geometric configurations (inline and staggered arrangements, and two longitudinal distances between tubes). Consequently, two-dimensional numerical calculations represent three-dimensional numerical calculations. The URans method is used to model turbulence. Consequently, three distinct types of turbulence models are employed. There are comparisons between three distinct turbulence models and experimental data.

### PROBLEM DEFINITION

Figure 1 depicts the experimental configuration. The test section's channel is made of Plexiglas material. It has an inner rectangular cross section with dimensions of 90 mm by 100 mm and a wall thickness of 5 mm. The length of the channel inlet is determined to be 1410 mm in order to provide a fully developed flow zone for the Reynolds numbers considered. At the channel inlet, four pressure sockets are used. Air is used as a fluid, and it enters the channel at speeds ranging from 0.26 to 1.31 metres per second.

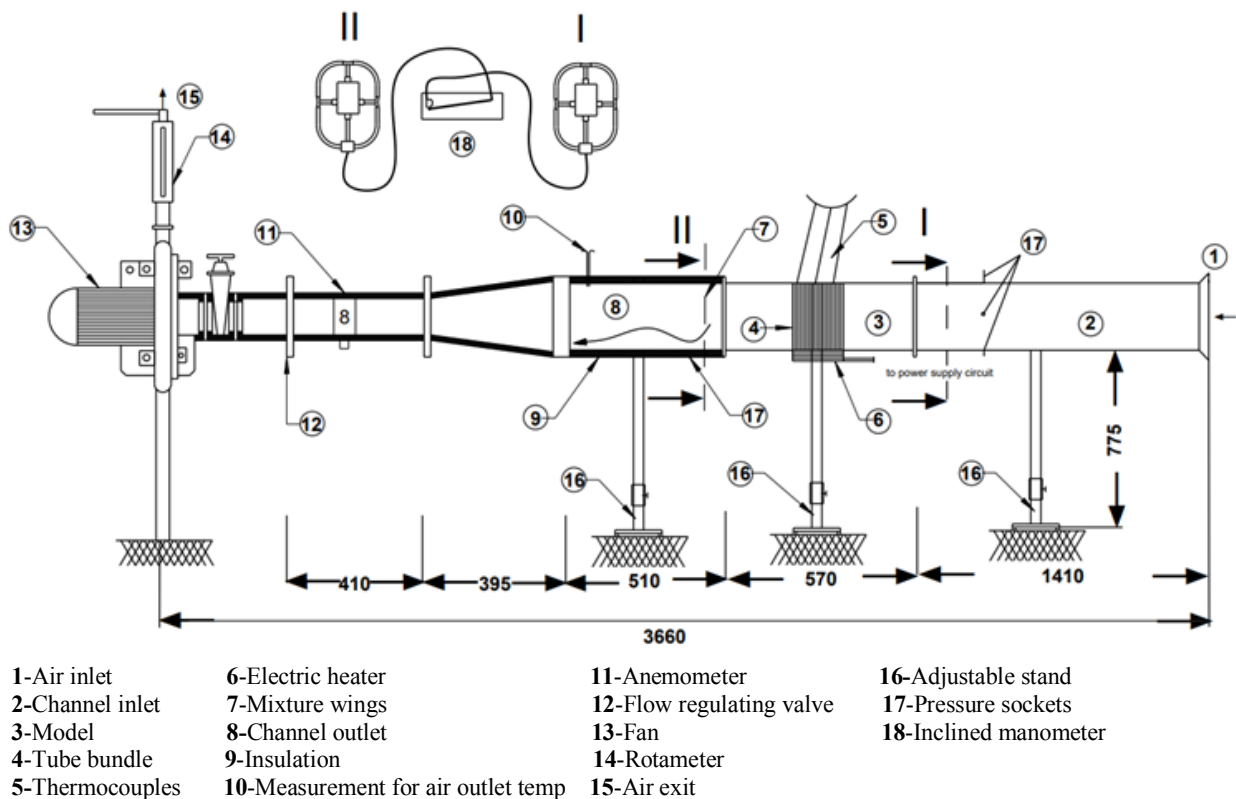


Figure 1. Schematic diagram of the experimental setup.

The tubes are 140 mm in length and constructed from mahogany, which has a low thermal conductivity. The tubes are hollow, and thermocouples are located within the tube walls to measure the temperature of the fluid. As was previously stated, steel support plates are utilised at the base of the model. Using different voltage and current values, the steel support plate is heated unilaterally by the electric resistance method, ensuring a primarily constant heat flux. Since mahogany is deformed at higher heat fluxes, values of 96 for heat flux indicate deformation.

It is applied  $W/m^2$ , 88.5  $W/m^2$ , and 86.25  $W/m^2$ . To homogenise the heat flux, an aluminium plate with a perforation is used.

Under a steel plate is an aluminium plate with a thickness of 2 mm; the heaters are attached to this aluminium plate. As a heater, copper–nickel wires are utilised. Ceramic fibre with a thickness of 3 mm and aluminum-coated glass wool with a thickness of 50 mm were used, respectively, to prevent heat loss from heaters.

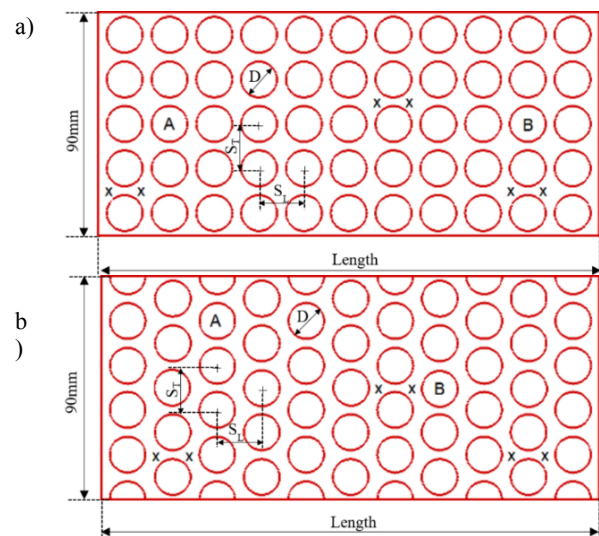
The 570 mm long test section containing the tube bundles is positioned in the middle of the channel. Over the support plate, the tube bundle can be arranged inline or staggered. A support plate is fabricated from steel. In this diagram, inline and staggered tube bundles are depicted.

Fig 2. 5 x 11 rows (transverse x longitudinal) were used to construct the tube arrays. 90 millimetres was the height of the support plate. The arrangement is defined by the tube diameter (D), the transverse distance (ST), the longitudinal distance (SL), and the length of the support plate (L). The diameter of the tube is 14.4 mm. The tube has a height-to-diameter ratio of 9.72. While the transverse distance is assumed to be 18 mm, two different longitudinal distances of 18 mm and 21.6 mm are used. The length of the support plate varies with the distance between the rows along its longitudinal axis. For the 18 mm and 21.6 mm longitudinal distances, support plate lengths of 196.4 mm and 232.4 mm are used, respectively. Table 1 lists the Reynolds number based on inlet velocity and hydraulic diameter. Keeping the Prandtl number at 0.7.

Following the section containing the tube bundles is a 510-mm-long outlet section with four pressure sockets, similar to the channel's inlet section. To achieve a uniform temperature at the channel outlet, a combination of wings is utilised.

Temperature is measured via Nickel chromium – Nickel (NiCr-Ni) thermocouples at eighteen points. In Fig 2, a

mark “A”, “B”, and “x” represent the fluid and support plate temperature points, respectively. The distances between the temperature markings on the support plate and the nearest tube surface were 2 mm. The thermocouples' diameter was 0.2 mm. Three millimetres outside of the tubes, thermocouples are passed through the tubes to measure fluid temperature. All thermocouples are positioned so as not to impede fluid flow. Using a two-channel scanner, the temperature of eighteen points is measured. The reference temperature is 0 degrees Celsius, which is maintained by ice water in a thermos bottle. A digital thermometer with high sensitivity between -50°C and 50°C is used to control the temperature of ice water. Two rotameters are utilised for flow measurement. Both ends of the fan outlet are equipped with rotameters. It is assumed that two rotameters pass identical amounts of air.



**Figure 2.** Tube bundle arrangements over the steel support plate (a) inline (b) staggered

A rotameter's measuring lines were calibrated with reference to 760 mmHg pressure and 20°C temperature. Flow velocity is measured with an anemometer, and the resulting flow rate is compared to rotameter readings. Flow regulating valves are installed to control the flow rate and, consequently, the Reynolds number. 4% is the turbulent intensity of flow. With the aid of pressure sockets at the channel inlet and outlet, the pressure drop values of various Reynolds numbers in the tube bundle are determined. The used inclined manometer has 14 mmH<sub>2</sub>O measurement capability and it works with alcohol with a density of 0.850 kg/m<sup>3</sup>. Connections between inclined manometer and measurement points support with equal length hoses.

**Table 1.** The used Reynolds numbers for all longitudinal distances and arrangements.

		1	2	3	4	5	6	7	8
S <sub>L</sub> =18	inline	989	1505	2026	2751	3672	4313	5139	-
	staggered	1508	1714	2229	3054	4097	4830	5550	-
S <sub>L</sub> =21.6	inline	1058	1828	2550	3323	4115	4933	5541	-
	staggered	1066	1838	2547	3287	4057	4826	5618	6352

Using a differential approach to error analysis, a comprehensive analysis of experimental uncertainties is conducted (Holman, 1994). The maximum uncertainty values in the measured measurement parameters are temperature  $\pm 1.18\%$ , air velocity in the tubes and pressure drop through the model  $\pm 3.42\%$ ,  $\pm 1.03\%$ . The maximum uncertainties for Reynolds number, Nusselt number are found to be  $\pm 1.28\%$  and  $\pm 3.02\%$  respectively.

Between the support plate and air, the convective heat transfer coefficient ( $h$ ) of the support plate and the air was counted up as;

$$Q = \dot{m} \cdot C_p \cdot (T_i - T_0) = h \cdot F_{WA} \cdot \left( T_w - \frac{T_i + T_0}{2} \right) \quad (1)$$

where  $Q$  indicates the heat flow rate,  $\dot{m}$  the mass flow rate,  $T_i$  the inlet temperature,  $T_0$  outlet temperature,  $T_w$  the average wall temperature and  $F_{WA}$  the heat transfer area. In order to find the average wall temperature, the temperature was measured at six different points on the support plate and the arithmetic mean was taken. The points used are indicated by x in Fig 2. The Nusselt number based on tube diameter is, then, calculated as;

$$Nu = \frac{h \cdot D}{k} \quad (2)$$

where  $k$  denotes the fluid thermal conductivity. As mentioned before, the pressure values are measured via pressure sockets at the channel inlet and outlet. The difference in these pressure values gives the pressure drop ( $\Delta P$ ). With using pressure drops, the friction factor is determined as;

$$f = \frac{\frac{\Delta P}{dx} \cdot D}{\frac{1}{2} \cdot \rho \cdot U^2} \quad (3)$$

where  $\rho$  is the fluid density,  $U$  is inlet velocity, and  $dx$  denotes the distances between pressure sockets. Finally, the area goodness factor for thermohydraulic performance is introduced (Kuppan, 2000). The area goodness factor was calculated by dividing the Colburn j-factor by the friction factor.

$$A_{GF} = \frac{Nu}{Re \cdot Pr^{\frac{1}{3}} \cdot f} \quad (4)$$

where  $Re$  and  $Pr$  denote Reynolds number and Prandtl number, respectively.

## Modeling

### Turbulence modeling

The numerical analysis is performed using the commercial code Ansys-Fluent (2009), which is based on FVM. The flow must be time-dependent and turbulent within this Reynolds number range (Aslan et al., 2015; Aslan, 2016). For modelling turbulence, a URANS approach is adopted, for being able to capture flow large scale unsteadiness that can occur in the wake of the

cylinders. In the previous investigation (Aslan, 2016), four different turbulence models were used which were Realizable  $k-\epsilon$ ,  $k-\omega$ , SST (Shear Stress Transport), and transition SST. According to previous investigations, Realizable  $k-\epsilon$  predictions were far from experimental results, therefore, the remaining three turbulence models except the Realizable  $k-\epsilon$  turbulence model are used in the present investigation. Here,  $k$  is turbulent kinetic energy,  $\omega$  is specific dissipation rate (Ansys-Fluent, 2009).

**Table 2.** The used number of cells of quarter modelling strategy

	<b>Inline</b>	<b>Staggered</b>
$S_L=18\text{mm}$	6 703 251	6 632 314
$S_L=21.6\text{mm}$	8 313 400	8 313 300

Wilcox (1998) developed the  $k-\omega$  model, with modifications for low Reynolds number effects, compressibility, and shear flow dispersion. Sensitivity to turbulence values and specific rate of dispersion except for the shear layer are powerless points of the Wilcox  $k-\omega$  model. For addressing these weak points, Menter (1994) developed the SST turbulence model. Accordingly, the correct formulation in the near wall region (Ansys, 2009) of the  $k-\omega$  model was effectively blended with the robust behavior of the  $k-\epsilon$  model (Launder and Spalding, 1974) in the free stream, where  $\epsilon$  is the dissipation rate. Combining the SST turbulence model with two other transport equations from the perspective of momentum thickness Reynolds number, which are for intermittency and the transition onset criteria, a new turbulence model, transition SST, has emerged (Menter et al., 2003; Menter et al., 2004; Lotfi et al., 2014). Near-wall turbulence models are not modelled using the wall function approach (Durbin and Reif, 2011). If the grid resolution is sufficient, the used turbulence equations can represent turbulence close to the wall. When designing the grid, attention was paid to the fact that the  $y^+$  (Ansys-Fluent, 2009) value of the non-dimensional wall distance of the cells near the wall was always below 1.

### The boundary conditions

To reduce computational effort, two-dimensional numerical analyses are performed to represent three-dimensional numerical analyses using proportion coefficients, as will be described in greater detail below.

There were three distinct preliminary investigations conducted to determine proportion coefficients. In the first preliminary study, a single tube was considered in the channel, and a three-dimensional numerical study was conducted. The strategy for modelling is based on full and semi-models. A symmetric half-length boundary condition was applied to the tube's half-length modelling. Practical examination revealed no difference between the full and half models (less than 1% deviation in Nusselt number). Thus, it was determined that applying the symmetrical boundary condition in half tube length (the  $xy$  plane) would not raise any objections. In the second preliminary analysis, a tube bundle was utilised rather

than a single tube, and the flow characteristics of all tubes were examined in two dimensions. Again, both full and half modelling approaches were employed. The symmetry boundary condition utilised in the half model was placed in the centre of the side walls. Due to these comparisons, it was realised that there was no practical difference between the time-averaged results of full and half models, and that the symmetry boundary condition could be applied to the xz plane. Note that this symmetry boundary is perpendicular to the one used in the first preliminary study, so that a quarter of the domain is bounded by two symmetry planes. In the third preliminary study, a numerical investigation of a single tube in a channel in two-dimensional domains was conducted. On the tube wall, two different heat fluxes were applied. The Nusselt number of two distinct heat flux analyses was nearly identical, with only a 1% difference observed. Therefore, it can be concluded that flow characteristics, and not necessarily thermal boundary conditions, play a significant role in determining the Nusselt number.

In accordance with the first and second preliminary validations, a quarter of the channel volume is used as the solution domain in the three-dimensional calculations, which is bounded by two channel walls and two symmetry planes, as depicted in Figure 3. The number of cells in three-dimensional grids is displayed in Table 2. Only for the highest Reynolds number and with the SST turbulence model was a three-dimensional analysis with quarter modelling performed.

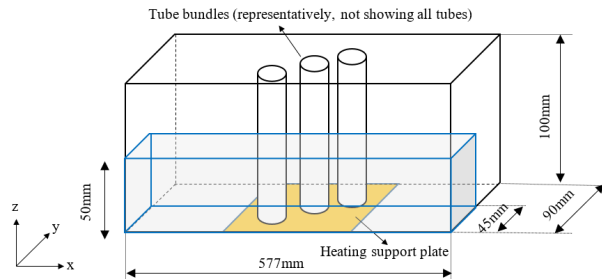


**Figure 3.** The schematic of quarter modelling strategy with indication of coordinate system

The velocity fields around a cylinder are predicted utilising a two-dimensional half domain with symmetric boundary conditions. While the actual problem involves heat transfer through supporting plates with constant heat flux, the absence of supporting plates in the 2D numerical computations makes it possible to apply constant heat flux to the cylinders. The focus is on capturing the flow characteristics in order to predict the Nusselt number, according to a third preliminary validation. Due to the absence of the third dimension, there are minor differences between three-dimensional and two-dimensional flow characteristics. However, the overall flow behaviour, including flow separation and the formation of von Karman vortex streets, can be observed in both cases.

According to the second preliminary investigation, a constant heat flux is applied to the cylinders in the

absence of a supporting plate. In light of the third preliminary, the constant heat flux is not decisive for the prediction of the Nusselt number. Obviously, in two-dimensional numerical calculations, an equivalent heat flux value must be defined for three-dimensional numerical calculations to accurately determine the outlet temperature. If we combine the second (due to determining equivalent constant heat flux at the cylinders) and third (due to the significance of flow characteristics for Nusselt number predictions), preliminary validation two-dimensional numerical computations can be transferred to three-dimensional numerical computations by means of a constant coefficient.

Taking into account the quarter domain described previously, the computational work for a three-dimensional calculation is reduced by a factor of four. Nonetheless, the computational effort required for a three-dimensional calculation is considerable. Due to the large number of tubes and high grid resolution, this is the case. Consequently, it was necessary to find an additional method for performing parametric studies with reasonable effort and time. To accomplish this, the so-called "proportion coefficient" method is utilised. The idea behind this concept is that, for a given geometry, the ratio between the two-dimensional and three-dimensional results remains constant, as expressed by a "proportion coefficient" that is independent of the Reynolds number. Comparing the two-dimensional and three-dimensional results for a single Reynolds number enables the calculation and application of proportion coefficients for different Reynolds numbers. This indicates that, for the remaining cases (Reynolds numbers), three-dimensional calculations are not required. Calculations can be performed in two dimensions and then transferred to three dimensions using proportion coefficients previously determined.

Thus, for obtaining the proportion coefficients, three and two-dimensional calculations are performed for inline and staggered configurations, for two different longitudinal distances ( $S_L = 18$  mm,  $S_L = 21.6$  mm), for a single Reynolds number. To achieve this, the highest Reynolds number is used as a starting point, and three-dimensional results for the quarter domain are obtained. Utilising the SST turbulence model. Comparing the two-dimensional and three-dimensional results yields the proportion coefficients, which are then used to convert the two-dimensional Reynolds numbers to three-dimensional. The proportion coefficients are assumed to be independent of the turbulence model used. Formally, the proportion coefficients were expressed. The obtained proportion coefficients are listed in Table 3.

for the Nusselt number ;

$$Nu_{proportion} = \frac{Nu_{2D}}{Nu_{3D}} \quad (5)$$

the pressure drop;

$$\Delta P_{proportion} = \frac{\Delta P_{2D}}{\Delta P_{3D}} \quad (6)$$

**Table 3.** The proportion coefficients

		<b>Inline</b>	<b>Staggered</b>
$S_L = 18 \text{ mm}$	Nu	1.18	1.16
	$\Delta P$	0.60	0.91
$S_T = 21.6 \text{ mm}$	Nu	1.19	1.21
	$\Delta P$	0.79	0.82

Figure 4 depicts the two-dimensional domains employed. In the inlet section (channel inlet, Fig. 1), preliminary calculations determine the velocity and turbulence rates. The distributions at the exit of the channel entrance are defined as the main solution field's entrance boundary conditions. The input is maintained at a constant temperature due to the energy equation. For all

convective-diffusive transport variables, the zero gradient boundary condition at the output of the solution field is applied, i.e., the outflow boundary condition is used. Momentum equations in walls are applied with a non-slip boundary. For the energy equation, adiabatic boundary conditions are applied to all walls, with the exception of tube bundles. In three-dimensional analyses, a uniform heat flux boundary condition is prescribed at the support plate, whereas in two-dimensional analyses, a constant heat flux is applied to the tube surfaces. According to the heat flux in three-dimensional domains, the heat flux in two-dimensional domains is calculated equivalently. Consequently, outlet temperatures are obtained that are comparable for both two- and three-dimensional domains.

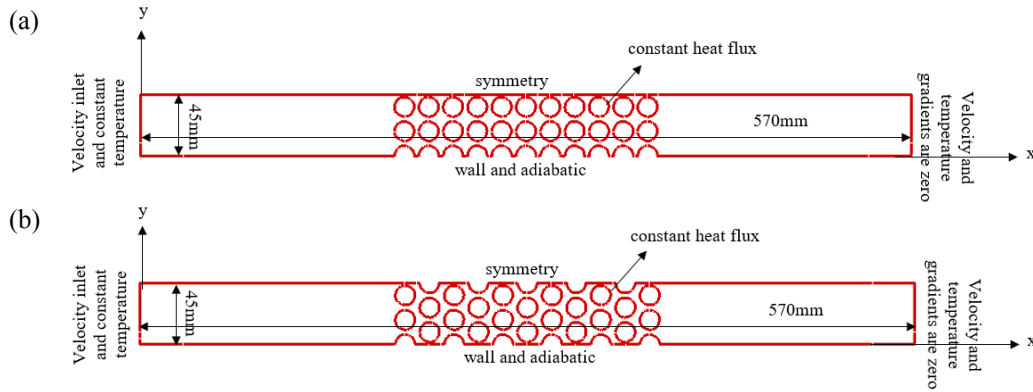


**Figure 4.** Two-dimensional domains with boundary conditions for (a) inline and (b) staggered arrangements

Before determining the equivalent heat flux in a two-dimensional domain, the total heat in a three-dimensional domain must be determined. Multiple heat flux and heat transfer surface area at the support plate are used to calculate total heat. When the total area of the support plate is subtracted from the total area of the tubes, the heat transfer area at the support plate is obtained. Second, the total heat is partitioned into two-dimensional domains based on the area of all tubes. The area of all tubes is determined by multiplying the perimeter of all tubes by the channel height (100 mm). For all two- and three-dimensional calculations, the turbulent intensity and length scale are 4% and one-third of the hydraulic diameter, respectively.

### The grids of numerical modeling

Abed and Afgan (2017) used the FVM for spatial discretization with second-order upwind to convection terms. For time integration, an implicit second-order scheme is used. For pressure velocity coupling, the PISO algorithm is utilised (Ansys, 2009). Default under-relaxation factors which are pressure is 0.3, momentum is 0.7, turbulent quantities are 0.8 and energy is 1.0 are used (Abed and Afgan, 2017). For all equations except the

energy equation, a  $10^{-6}$  residual value is required as a convergence factor. The residual value  $10^{-8}$  is necessary for the convergence factor of energy equations. Structured and unstructured mesh strategies are used concurrently in 2-D numerical calculations. In close proximity to the wall, structural topologies are utilised, whereas unstructured topologies are employed in distant areas. Structured grids (boundary layer meshes) are utilised in remote regions near the bottom walls.

In remote areas, we believe that using an unstructured grid with boundary layer meshes provides the same level of accuracy as using a multiblock structured grid. A grid independence study was not conducted to determine mesh resolutions; however, the authors' prior work was utilised. Benim et al. (2008) investigated the flow through a circular cylinder using the LES, DES, RANS, and URANS methods. In this study, the circumference of the cylinder was distinguished between two- and three-dimensional calculations using 240 cells. According to Benim et al. (2008), the meshes employed are adequate for accurately predicting flow characteristics such as drag and pressure coefficients. Different aspects of the produce grids are represented in Fig 5, for arrangements of (a)  $S_L = 18 \text{ mm}$ , inline, (b)  $S_L = 18 \text{ mm}$ , staggered, (c)  $S_L = 21.6 \text{ mm}$ , inline, and (d)  $S_L = 21.6 \text{ mm}$ , staggered.

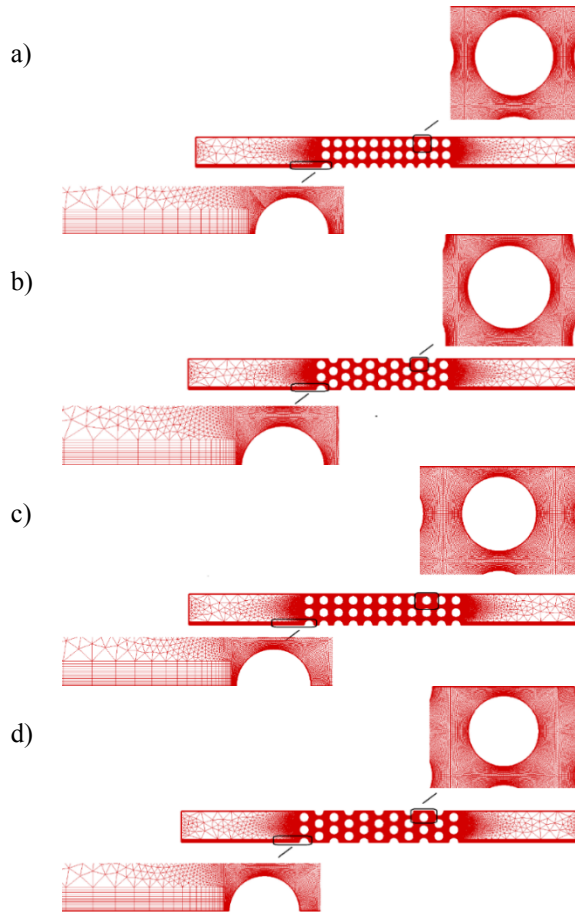


**Figure 5.** Two dimensional meshes for (a)  $S_L=18\text{mm}$ , in-line, (b)  $S_L=18\text{mm}$ , staggered, (c)  $S_L=21.6\text{mm}$ , in-line, (d)  $S_L=21.6\text{mm}$ , staggered

In Table 4, the simulation's employed cell numbers are listed. For the three-dimensional numerical computations, the same mesh strategy as in the two-dimensional case is utilised, with the addition of 72 cells in the third direction. This expanded mesh configuration permits a comprehensive representation of the three-dimensional flow behaviour and allows for more precise predictions of the flow characteristics and heat transfer phenomena.

**Table 4.** The used number of cells of two-dimensional domain

	<b>Inline</b>	<b>Staggered</b>
$S_L = 18 \text{ mm}$	150 049	149 908
$S_T = 21.6 \text{ mm}$	150 666	150 666

In transient computation, the time step size has been selected in such a way that the cell Courant number takes a value about one. Drag and lift coefficients are monitored with time for four tubes. Two of four tubes (tube-1 and tube-2) are located on inlet side of the model, and the other two tubes (tube-3 and tube-4) are placed on exit side of the model. By looking at the drag and lift coefficients, the oscillation frequency or periods for each tube are determined. Time averaged values, which are x-velocity, y-velocity, pressure and temperature, are determined according to largest oscillation period. Using

these time-averaged values, Nusselt number (Eq.1 and Eq.2), friction factor (Eq.3) and area goodness factor (Eq.4) are determined.

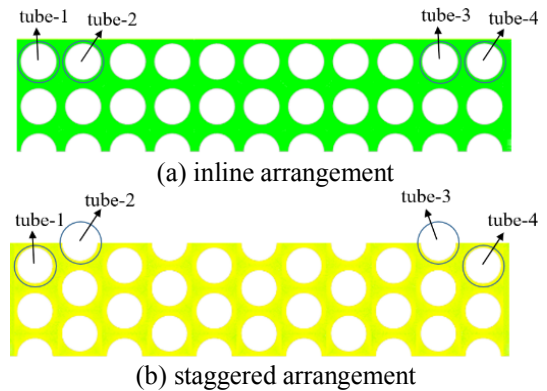


**Figure 6.** The monitored tubes for drag and lift coefficient and for (a) in-line and (b) staggered arrangements.

## RESULTS AND DISCUSSIONS

The numerical calculations included Reynolds values between 989 and 6352. Across all employed turbulence models, qualitative flow characteristics remained remarkably consistent. In light of this, only the predictions derived from the SST turbulence model will be considered in the initial section discussing the general flow characteristics. At the conclusion of this section, a quantitative comparison of the predicted Nusselt number, friction factor, and area goodness factor will be carried out, incorporating the results obtained from the various turbulence models utilised. This comparative analysis will shed light on the performance and precision of the various turbulence models in predicting the heat transfer and flow characteristics of the system.

In Fig 7, the time-averaged x-velocity distributions are shown for (a)  $S_L=18 \text{ mm}$ , in-line, (b)  $S_L=18 \text{ mm}$ , staggered, (c)  $S_L=21.6 \text{ mm}$ , in-line, and (d)  $S_L=21.6 \text{ mm}$ , staggered configurations. At the highest Reynolds number, the distribution of time-averaged x-velocity is presented for each configuration. Flow patterns before tube bundles have not changed significantly in any of four configurations due to the fully developed velocity at the model's inlet. In the tube bundle, the flow strip in the in-line is in the form of a linear line. Streams originating from a single source are always divided into two for staggered arrangement. Maximum time average x velocities are found between the tube rows in both configurations. Behind the initial row, the flow pattern produces an extremely repetitive pattern. In the streams surrounding the cylinders, von Karman's vortex street (instable vortex shedding) is observed. This is due to the fact that the back of the rollers have varying Reynolds numbers and modes. Due to the extremely close spacing between cylinders within the tube bundles, this behaviour is dampened. The time-averaged axial velocity regions reveal a low-velocity zone where the main flow is drawn towards the side wall in the middle of the channel (it clears the symmetry plane). This is possible because the jet acts as an ejector between the side wall and the next

cylinder, drawing fluid from the surrounding environment. In Fig 8 these are shown the time-averaged pressure distributions for (a)  $S_L=18$  mm, inline, (b)  $S_L=18$  mm, staggered, (c)  $S_L=21.6$  mm, inline, and (d)  $S_L=21.6$  mm, staggered configurations. Again, time-averaged

pressure distributions at the highest Reynolds numbers are presented in Fig 8 for each configuration. Significant pressure variations can be achieved for all configurations. Staggered arrangements and small longitudinal distance ( $S_L=18$  mm) produce higher pressure drop values.

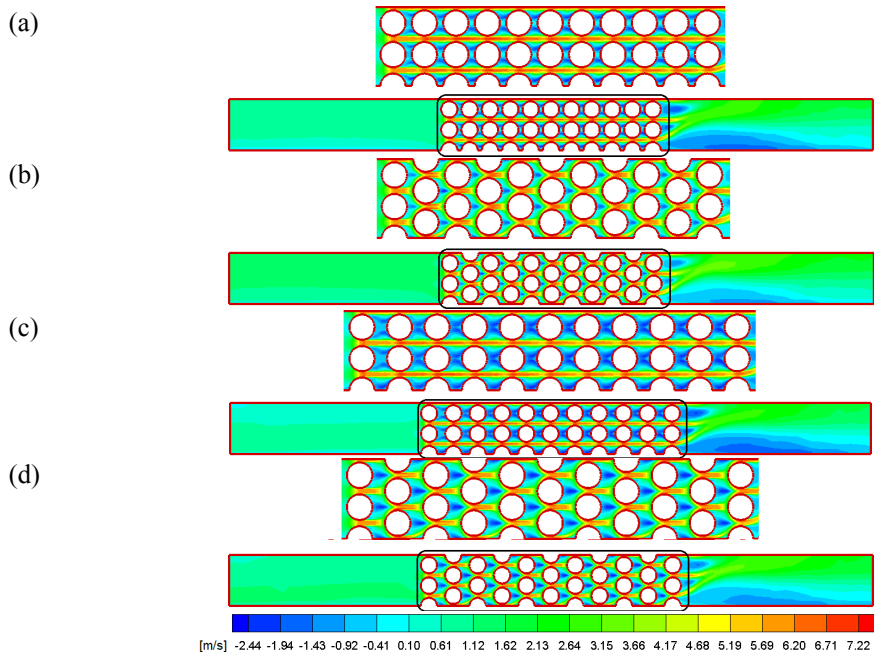


**Figure 7.** The SST predictions of time-averaged x-velocity distributions for (a)  $S_L=18$ mm, inline ( $Re = 5139$ ), (b)  $S_L=18$ mm, staggered ( $Re = 5550$ ), (c)  $S_L=21.6$ mm, inline ( $Re = 5541$ ) and (d)  $S_L=21.6$ mm, staggered ( $Re = 6352$ )

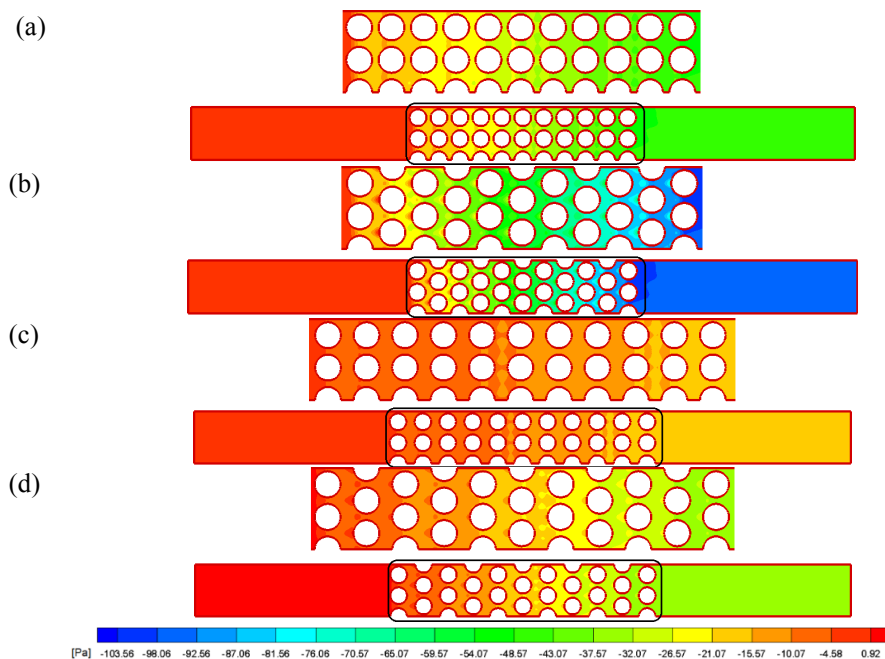


**Figure 8.** The SST predictions of time-averaged pressure distributions for (a)  $S_L=18$  mm inline ( $Re=5139$ ), (b)  $S_L=18$  mm staggered ( $Re=5550$ ), (c)  $S_L=21.6$  mm inline ( $Re=5541$ ) and (d)  $S_L=21.6$  mm staggered ( $Re=6352$ )

Time-averaged temperature distributions are presented in Fig 9 for (a)  $S_L=18$  mm, inline, (b)  $S_L=18$  mm, staggered,

(c)  $S_L=21.6$  mm, inline, and (d)  $S_L=21.6$  mm, staggered configurations. Estimates of the time-averaged

temperatures are displayed for all configurations at the highest Reynolds numbers. With a constant heat flux, the temperature of the cold fluid entering the model gradually rises for all configurations. There is a recirculation zone behind the tubes where warmer zones can be observed. Nusselt numbers are derived from the time-averaged results of an experiment and a numerical analysis.

Fig 10 shows the measured and calculated Nusselt numbers (Nu) as a function of Reynolds number (Re) for the configurations of (a)  $S_L=18$  mm, inline (Aslan,2016), (b)  $S_L=18$  mm, staggered (Aslan,2016), (c)  $S_L=21.6$  mm, inline, and (d)  $S_L=21.6$  mm staggered. As the Reynolds number increases, flow characteristics become more

turbulent, as expected, the Nusselt numbers of experiments and numerical predictions increase with the Reynolds number. For staggered arrangements, streams from a row one are always divided into the next two (see Figure 7), therefore temperature gradients at near cylinders of staggered arrangements are greater than temperature gradients at near cylinders of inline arrangements. Nusselt numbers in the staggered arrangements [Fig 10(b) and Fig 10(d)] are higher than the inline arrangements [Fig 10(a) and Fig 10(c)], for both longitudinal distances.

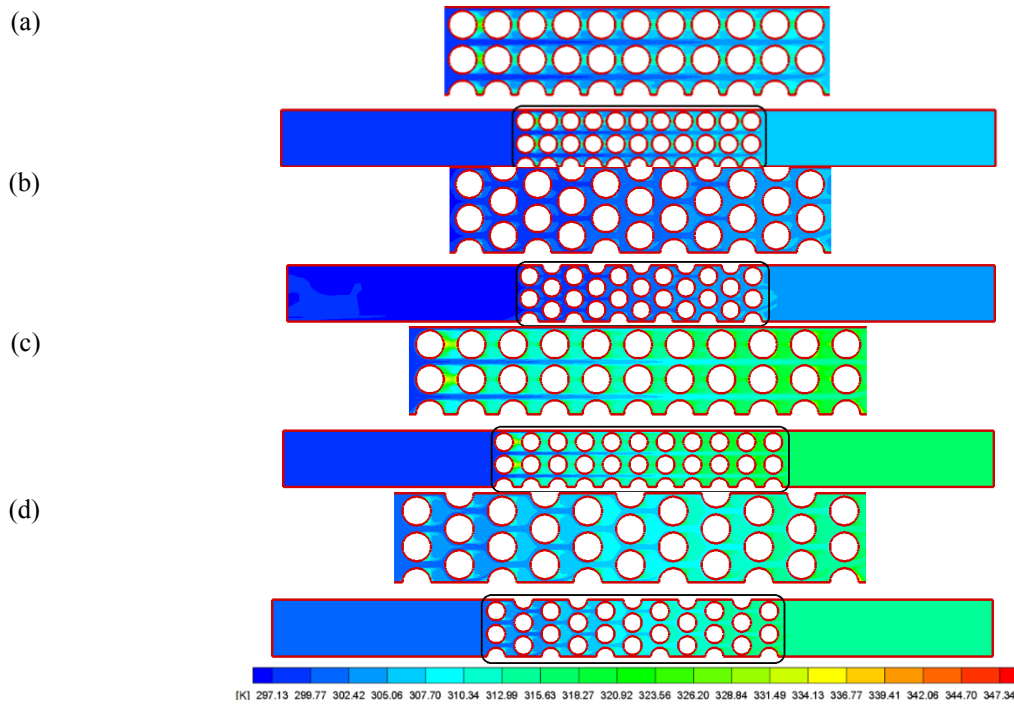


**Figure 9.** The SST predictions of time-averaged temperature distributions for (a)  $S_L=18$  mm inline ( $Re=5139$ ), (b)  $S_L=18$  mm staggered ( $Re=5550$ ), (c)  $S_L=21.6$  mm inline ( $Re=5541$ ) and (d)  $S_L=21.6$  mm staggered ( $Re = 6352$ )

Furthermore, higher Nusselt numbers are observed to occur for the smaller longitudinal distance ( $S_L = 18$  mm) for both arrangements [Fig 10(a) and Fig 10(b)].

At a small longitudinal distance ( $SL = 18mm$ ), the flow behind the tube experiences the presence of adjacent tubes without undergoing complete mixing. Consequently, there is a greater degree of flow mixing than in cases where the tube distances are greater. This phenomenon occurs due to the close proximity of the tubes, which causes interactions and flow pattern disturbances. Incomplete mixing at shorter tube distances can have substantial effects on heat transfer and fluid dynamics, influencing variables such as the Nusselt number and flow characteristics. In order to gain a comprehensive understanding of the system's performance and optimise heat transfer efficiency, it is necessary to consider and analyse the flow behaviour at different longitudinal distances. Accordingly, larger temperature gradients occur at smaller longitudinal distances. For both arrangements of  $S_L = 18$  mm, the SST turbulence model predicts the nearest results to the

measurements. For the inline arrangement of  $S_L = 18$  mm, under and over predictions are observed for the  $k-\omega$  and transition SST turbulence models, respectively [Fig 10(a)]. The prediction of the  $k-\omega$  turbulence model is not very good, particularly at high Reynolds numbers for the staggered arrangement of  $S_L=18$  mm [Fig 10(b)]. For the long longitudinal distance ( $S_L=21.6$  mm) of the inline arrangement, the SST and  $k-\omega$  turbulence models predict analogous results, which are quite near to the experimental result, while predictions of transition SST are also found reasonable [Fig 10(c)]. Over predictions are observed for all turbulence models in the staggered arrangement of the long longitudinal distance ( $S_L=21.6$  mm) [Fig 10(d)]. The utilization of a long longitudinal distance ( $SL=21.6$  mm) facilitates a greater presence of free stream flow around the tube, which impacts the heat transfer characteristics. In comparison to experimental results, the SST turbulence model tends to overestimate the Nusselt number. At low Reynolds numbers, this overestimation is especially pronounced. Notable similarities exist between the predictions of all

turbulence models, particularly at low Reynolds numbers. This suggests that the choice of turbulence model has less of an effect on the predictions when Reynolds numbers are low. As the Reynolds number rises, however, the disparities between the turbulence models become more pronounced. When analysing heat transfer performance and predicting the Nusselt number, it is crucial to consider the appropriate turbulence model and the effect of Reynolds numbers on the precision of predictions.

Friction factor as a function of Reynolds number is shown for the configurations (a)  $S_L=18$  mm, inline (Aslan,2016), (b)  $S_L=18$  mm, staggered (Aslan,2016), number (c)  $S_L=21.6$  mm, inline and (d)  $S_L=21.6$  mm,

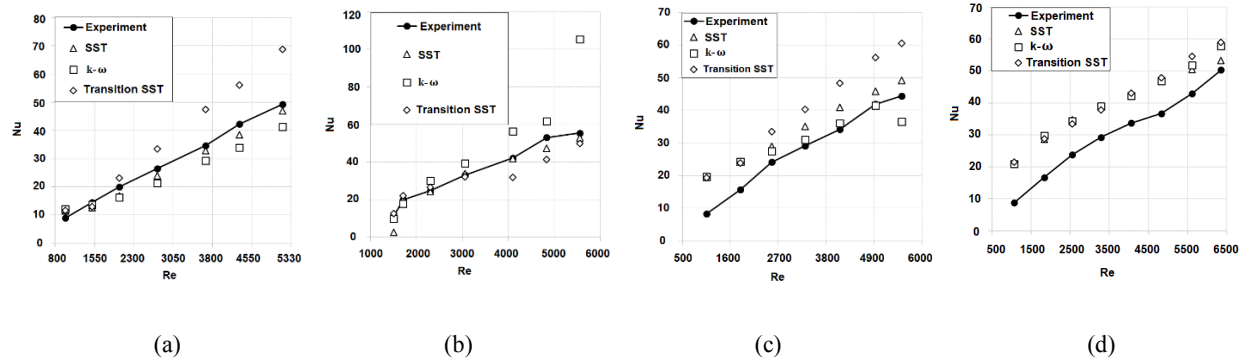


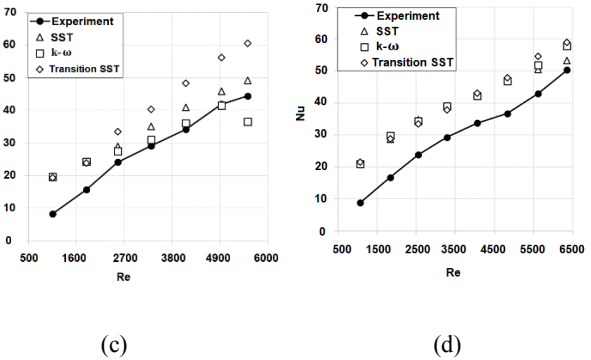
**Figure 10.** Nusselt number as a function of Reynolds number (a)  $S_L=18$ mm, inline, (b)  $S_L=18$ mm, staggered, (c)  $S_L=21.6$ mm, inline, and (d)  $S_L=21.6$ mm, staggered

Predictions of the SST turbulence model is quite good according to experiment result for both arrangements of  $S_L=18$  mm, whereas the other turbulence models also perform reasonably well [Fig 11(a) and Fig 11(b)].

The estimation of the transition SST model is so close to experimental results for the inline arrangement of  $S_L=21.6$  mm. SST and k- $\omega$  turbulence models predict quite well at low Reynolds numbers. However, with increasing Reynolds number, predictions of SST and k- $\omega$  turbulence models are far from experiments. For the staggered arrangement of  $S_L=21.6$  mm, all turbulence models behave similarly, and their predictions are quite good compared to the experimental results [Fig 11(d)]. However, some deviations are observed at high Reynolds numbers.

Convective heat transfer and pressure drop are not taken into account separately when designing heat exchangers. Both are considered concurrently. Consequently, a new parameter titled area goodness factors is created. The ratio of Colburn factor  $j$  to friction factor is the area goodness factor. If the performance value is high, convective heat transfer will be high and the friction factor will be low, resulting in efficient heat transfer and low operating costs. Fig 12 presents the measured and predicted area goodness factor as a function of the Reynolds number for the configurations of (a)  $S_L=18$  mm, inline (Aslan,2016), (b)  $S_L=18$  mm, staggered

staggered in Figure 11. As expected, friction factors increase for all configurations as pressure drop increases more than dynamic pressure as Reynolds number increases. At both longitudinal distances, the friction factor values for staggered arrangements are greater than those for inline arrangements. This is because the pressure against the flow is greater in staggered configurations. In addition, as mentioned previously, the rising number of Nusselt is a result of this (Figure 10). As the longitudinal distance increases at the same Reynolds number, the pressure drop increases; consequently, the friction factor increases for both configurations as the longitudinal distance increases [Fig 11(c) and Fig 11(d)].



(Aslan,2016),(c)  $S_L=21.6$  mm, inline and (d)  $S_L=21.6$  mm, staggered. Time-averaged results from experiments are numerical calculation used to get the area goodness factor. Reynolds number decreases the area goodness factor for all configurations. In the case of small longitudinal distances, inline arrangement results in a greater area goodness factor than staggered arrangement. For long longitudinal distances, however, inline arrangement produces a lower area goodness factor than staggered arrangement. When we observe the inline arrangement, the area goodness factor of  $S_L=18$  mm is greater than the area goodness factor of  $S_L=21.6$  mm. In the same manner, when we look at the staggered arrangement, a small longitudinal distance ( $S_L=18$  mm) produces a bigger area goodness factor than a long longitudinal distance ( $S_L=21.6$  mm). For all cases, especially, for low Reynolds numbers, predictions of all turbulence models are not good enough, however, with increasing Reynolds numbers, turbulence model predictions are close to experimental results. For the inline arrangement of  $S_L=18$  mm [Fig 12(a)], the prediction of the SST turbulence model is close to experimental results after  $Re=1837$ . For the same arrangement and longitudinal distance, under and over-estimation are observed for k- $\omega$  and transition SST, respectively. For inline arrangement and staggered arrangement of  $S_L=21.6$  mm, all turbulence models behave similarly for a staggered arrangement of  $S_L=18$  mm [Fig 12(b)], prediction of transition SST turbulence models is quite good after  $Re=4057$ .

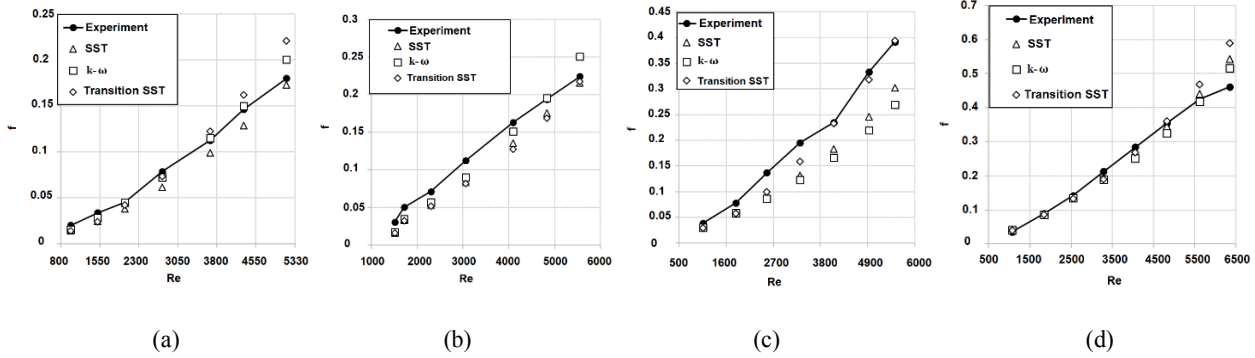


**Figure 11.** Friction factor as a function of Reynolds number (a)  $S_L=18\text{mm}$ , inline, (b)  $S_L=18\text{mm}$ , staggered (c)  $S_L=21.6\text{mm}$ , inline and (d)  $S_L=21.6\text{mm}$ , staggered

Generally, all turbulence models make over estimations for the same arrangement and longitudinal distance, only

prediction of the SST turbulence model is lower than experimental results at minimum Reynolds number.

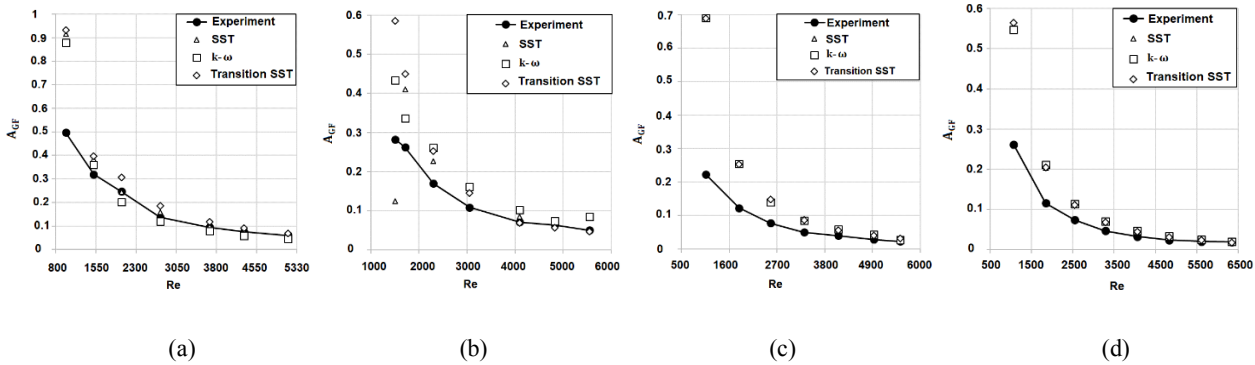


**Figure 12.** Area goodness factor as a function of Reynolds number (a)  $S_L=18\text{mm}$ , inline, (b)  $S_L=18\text{mm}$ , staggered (c)  $S_L=21.6\text{mm}$ , inline and (d)  $S_L=21.6\text{mm}$ , staggered

## CONCLUSIONS

This study examines the convective heat transfer and pressure drop characteristics of a heat exchanger with two different longitudinal distances ( $S_L=18\text{ mm}$  and  $S_L=21.6\text{ mm}$ ) and tube bundles arranged inline and staggered on supporting plates. Experimental and numerical methods are used to investigate these properties. The Reynolds numbers range from 989 to 6352, with a fixed Prandtl number of 0.7. Three turbulence models, namely  $k-\omega$ , SST, and transition SST, are utilized within the framework of the URANS approach. The experimental results serve as a benchmark for evaluating the precision of the numerical predictions.

To reduce the computational burden of large meshes, 2D calculations are performed instead of 3D calculations, and proportion coefficients are used to approximate the 3D behaviour based on the 2D results.

Across all geometric configurations, the Nusselt number and friction factor values are observed to increase with Reynolds number, while the area goodness factor decreases. The staggered configuration has a greater Nusselt number and friction factor than the inline configuration. Reducing the longitudinal distance between rows of tubes increases the Nusselt number but

decreases the pressure drop. For short longitudinal distances, the inline arrangement produces a greater area goodness factor than the staggered arrangement, whereas the opposite is true for long longitudinal distances.

In terms of turbulence models, the SST model provides the closest agreement with experimental results for both geometric patterns at small longitudinal distances. The  $k$ - and transition SST models also provide accurate forecasts. For the large longitudinal distance of the staggered arrangement, all turbulence models exhibit similar behaviour and are in excellent agreement with experimental data. In the case of the inline arrangement with a longitudinal distance of 21.6 mm, the  $k-\omega$  model performs best in predicting the Nusselt number, while the transition SST model provides the closest results for the friction factor. Lastly, for the inline configuration with a distance of 18 mm along the longitudinal axis, the SST model closely matches the experimental results for the area goodness factor.

## REFERENCES

Abed, N., and Afgan, I. (2017). A CFD study of flow quantities and heat transfer by changing a vertical to

- diameter ratio and horizontal to diameter ratio in inline tube banks using URANS turbulence models. *International Communications in Heat and Mass Transfer*, 89,18-30.
- Aburoma, M.M. , Cho, S.M., and Sawyer, R.H. (1975). *Thermal/hydraulic design considerations for Clinch River breeder reactor plant intermediate heat exchangers*, ASME, 75-WA/HT-101.
- Ansys-Fluent (2009) *Ansys-Fluent 12.0 User's Guide*. Ansys Inc.
- Aslan, E., Taymaz, I., Benim, A.C.(2015). Investigation of LBM curved boundary treatments for unsteady flows. *European Journal of Mechanics B/Fluids*,51,68-74
- Aslan, E. (2016). Numerical investigation of the heat transfer and pressure drop on the tube bundle support plates for inline and staggered arrangements. *Progress in Computational Fluid Dynamics*,56(1),38-47
- Barmasian, H.R., and Hassan, Y.A. (1997). Large eddy simulation of turbulent crossflow in the tube bundles. *Nuclear Engineering and Design*, 172,103-122.
- Beale, S.B., and Spalding, D.B. (1999). A numerical study of unsteady fluid flow in inline and staggered tube banks. *Journal of Fluids and Structures*,13,723-754.
- Benim, A.C., Cagan, M., and Gunes, D. (2004). Computational analysis of heat transfer in turbulent pipe flow. *International Journal of Thermal Science*, 43,725-732.
- Benim, A.C., Ozkan, K., Cagan, M., and Gunes, D. (2007). Computational investigation of turbulent jet impinging onto rotating disk. *International Journal of Numerical Methods for Heat and Fluid Flow*, 17, 284-301.
- Benim, A.C., Chattopadhyay, H., and Nahavandi, A. (2011). Computational analysis of turbulent forced convection in a channel with a triangular prism. *International Journal of Thermal Science*, 50,1973-1983.
- Benim, A.C., Brillert, D., and Cagan, M. (2004). Investigation into the computational analysis of direct-transfer pre-swirl systems for gas turbine cooling. *ASME Turbo Expo*,4,453-460.
- Benim,A.C., Geiger, M., Doehler, S., Schoenenberger ,M., and Roemer, H. (1995). Modelling the flow in the exhaust hood of steam turbines under consideration of turbine-exhaust hood interaction, in *Proc. 1st European. Conf. Turbomachinery - Fluid Dynamic and Thermodynamic Aspects: Computational Methods*,pp.343-357.
- Benim, A.C., Pasqualotto, E., and Suh, S.H. (2008). Modelling turbulent flow past a circular cylinder by RANS, URANS, LES and DES. *Progress in Computational Fluid Dynamics, An International Journal*,8,299-307.
- Bouris, D., Papadakis, G., and Bergeles, G. (2001). Numerical evaluation of alternate tube configurations for particle deposition rate reduction in heat exchanger tube bundles. *International Journal of Heat and Fluid Flow*, 22 ,525-536.
- Brandt, F. (1985). *Wärmeübertragung im Dampferzeugen und Wärmetauschen, FDBR-Fachverband Dampfkessel-Behälten-und Rohrleitungsbau*, Essen: Vulkan-Verlag.
- Chattopadhyay, H., and Benim, A.C. (2011). Turbulent heat transfer over a moving surface due to impinging slot jets. *Journal of Heat Transfer* ,133 ,104502-1.
- Dagsöz, A.K. Bestimmung des Wärmeübergangs an Rohrbündel Tragplatten für Fluchtende und Versetzte Rohraordnungen. ITU Makine Fakültesi Isı Tekniği ve Ekonomi Araştırma Kurumu Bülteni 1975; 13.
- Durbin, P.A., and Reif, B.A.P. (2011). *Statistical theory and modelling for turbulent flows*, (2nd ed.).Chichester,Wiley.
- Grimison,E.D. (1937). Correlation and utilization of new data on flow resistance and heat transfer for crossflow of gases over tube banks. *Trans. ASME*, 59,583-594.
- Hamid, M.O.A., Zhang, B., and Yang, L. (2014). Application of field synergy principle for optimization fluid flow and convective heat transfer in a tube bundle of a pre-heater. *Energy*,76, 241-253.
- Hilpert, R. (1933). *Wärmeabgabe von geheizten Drähten und Rohren im Luftstrom*. Fors. Ingenieurwesen,(4):215-224.
- Holman, J.P. (1994). *Experimental methods for engineers* (6th ed.).McGraw-Hill Int.
- Horvat, A., Leskovar, M., and Mayko, B. (2006). Comparison of heat transfer conditions in tube bundle cross-flow for different tube shaped. *International Journal of Heat and Mass Transfer*, 49 ,1027-1038.
- Ibrahim, T.A., and Goma, A. (2009). Thermal performance criteria of elliptic tube bundle in cross flow. *International Journal of Thermal Science* , 48 , 2148-2158.
- Khan, M.G., Fartaj, A., and Ting, D.S. (2004). An experimental characterization of cross-flow cooling of air via an in-line elliptical tube array. *International Journal of Heat Fluid Flow* ,25,636-648.
- Kukulka, D.J., and Smith, R (2014). Heat transfer evaluation of an enhanced heat transfer tube bundle. *Energy* ,75,97-103.

- Kuppan T. Heat exchanger design handbook. New York: Marcel Dekker Inc, 2000.
- Kwak, K.M., Torii, K., and Nishino, K. (2003). Heat transfer and pressure loss penalty for the number of tube rows of staggered finned-tube bundles with a single transverse row of winglets. *International Journal of Heat Mass Transactions*, 46, 175-180.
- Lauder, B.E., and Spalding, D.B. (1974). The numerical computation of turbulence flows. *Computer Methods Applied Mechanical Engineering*, 3,269-289.
- Lauder, B.E., and Massey, T.H. (1978).The numerical prediction of viscous flow and heat transfer in tube banks.*Journal of Heat Transfer*, 100,565-571.
- Lavasani, A.M., Bayat, H., and Maarefdoost, T. (2014). Experimental study of convective heat transfer from in-line cam shaped tube bank in crossflow. *Applied Thermal Engineering*, 65 ,85-93.
- Li, X., Zhu, D., Yin, Y., Liu, S., and Mo, X. (2018). Experimental study on heat transfer and pressure drop of twisted oval tube bundle in cross flow. *Experimental Thermal Fluid Science*, 99,251-258.
- Liao, L., and Liu, Z.H. (2011). Enhanced Boiling Heat Transfer of the Compact Staggered Tube Bundles under Sub-Atmospheric Pressures. *Heat Transfer Engineering* ,28,444-450.
- Lin, C.N., Liu, Y.W., and Leu, J.S. (2008). Heat Transfer and Fluid Flow Analysis for Plate-Fin and Oval Tube Heat Exchangers With Vortex Generators. *Heat Transfer Engineering* ,29,588-596.
- Lotfi, B., Zeng, M., Sunden, B., and Wang, Q. (2014). 3D numerical investigation of flow and heat transfer characteristics in smooth wavy fin-and-elliptical tube heat exchangers using new type vortex generators. *Energy* ,73,233-257.
- Maithani, R., Kumar, A., Zadeh, P.G., Safaei ,M.Z., and Gholamalizadeh, E. (2020). Empirical correlations development for heat transfer and friction factor of a solar rectangular air passage with spherical-shaped turbulence promoters. *Journal of Thermal Analysis and Calorimetry*, 139,1195–1212.
- Maqableh, A.M., Khadrawi, A.F., Al-Nimr, M.A., Ammoruah, S.A., and Benim, A.C. (2011). Heat transfer characteristics of parallel and counter flow micro-channel heat exchangers with varying wall resistance. *Progress in Computational Fluid Dynamics*, 11,318-328.
- Matos, R.S., Laursen, T.A., Vargas, J.V.C., and Bejan, A. (2004). Three-dimensional optimization of staggered finned circular and elliptic tubes in forced convection. *International Journal of Thermal Science*,43,447-487.
- Mavriodu, S.G., and Bouris, D.G. (2012). Numerical evaluation of a heat exchanger with inline tubes of different size for reduced fouling rates. *International Journal of Heat and Mass Transfer*, 55 ,5185-5195.
- Menter, F.R. (1994). Two equation eddy viscosity turbulence models for engineering applications. *AIAA Journal*, 32, 1598-1695.
- Menter, F.R., Kuntz, M., and Langtry, R.B., (2003). Ten years of experience with the SST turbulence model. *Heat and Mass Transfer*, 4,625-632.
- Menter, F.R., Langtry, R.B., Likki, S.R., Suzen, T.B., Huang, P.G., and Volker, S. (2006). A Correlation-Bases Transition Model Using Local Variables-Part-1: Model Formulation. *Journal of Turbomachinery*, 128 ,413-422.
- Mizushima, J., and Suehiro, N. (2005). Instability and transition of flow past two tandem circular cylinders. *Physics Fluids* ,14,104-107.
- Oclon, P., Lopata, S., Novak, M., and Benim, A.C. (2015). Numerical study on the effect of inner tube fouling on the thermal performance of high-temperature fin-and-tube heat exchanger. *Progress in Computational Fluid Dynamics* ,15,290-306.
- Oengoeren, A., and Ziada, S. (1992).Unsteady fluid forces acting on a square tube bundle in air cross-flow. in *Proc. 1992 International Symposium on Flow-Induced Vibration and Noise*,55-74.
- Ozturk, N.A., Ozalp, C., Canpolat, C., and Sahin, B. (2016). PIV measurement of flow through normal triangular cylinder arrays in the passage of a model plate-tube heat exchangers. *International Journal of Heat Fluid Flow* ,61(B),531-544.
- Pourdel, H., Afrouzi, H.H., Akbari, O.A., Miansari, M., Toghraie, D., Marzban, A., and Koveiti, A. (2019). Numerical investigation of turbulent flow and heat transfer in flat tube. *Journal of Thermal Analysis and Calorimetry*, 135,3471-3483.
- Taymaz, I., Aslan, E., and Benim, A.C. (2015). Numerical investigation of incompressible fluid flow and heat transfer across a bluff body in a channel flow. *Thermal Science*,19,537-547.
- Wilcox, D.C. (1988). *Turbulence Modelling for CFD*. DCW Industries.
- Yahiaoui, T., Ladjede, O., Imine, O. and Adjlout, L. (2016). Experimental and CFD investigations of turbulent cross flow in staggered tube bundle equipped with grooved cylinders. *J Braz Soc Mech Sci Eng*,38,163–175.
- You, Y., Xiao, S., Pan, N., and Deng, Z. (2017). Full Model Simulation of Shell side Thermal Augmentation

of Small Heat Exchanger with Two Tube Passes. *Heat Transfer Engineering*, 39,1024-1035.

Zhao, H., Liu, Z., Zhang, C., Guan, N., and Zhao, H. (2016). Pressure drop and friction factor of a rectangular channel with staggered mini pin fins of different shapes. *Experimental Thermal Fluid Science*, 71,57-69.

Zheng, Z., Yang, W., Cai, Y., Wang, Q., and Zeng, G. (2020). Dynamic simulation on ash deposition and heat transfer behavior on a staggered tube bundle under high-temperature conditions. *Energy*, 190,116390.



**Erman Aslan** received his B.Sc., M.Sc., and Ph.D. in Mechanical Engineering from Sakarya University. He was a researcher for his Ph.D. at Dusseldorf University of Applied Sciences, Germany. His research area is Lattice Boltzmann method, CFD, forced convection, aerodynamics and heat transfer. He is Associate Prof. at Kocaeli University.



**İmdat Taymaz** earned BSc degree in Mechanical Engineering from Istanbul Technical University in 1983. He got M.Sc. of Mechanical Engineering at ITU in 1985 and Ph.D. at Sakarya University in 2001. He has interest in the following research areas as internal combustion engines, alternative fuels, fuel cells, heat transfer. He is Professor at Sakarya University.



**Kemal Cakir** is Assistant Professor at Sakarya University. He got M.Sc. of Mechanical Engineering at ITU and Ph.D. at Sakarya University. His main research interest is experimental heat transfer.



**Elif Eker Kahveci** is Assistant Professor at Sakarya University. She received M.Sc. and Ph.D. in Mechanical Engineering from Sakarya University, Turkey. Her research is about fuel cells, CFD, heat transfer